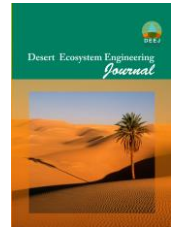




University of Kashan

Desert Ecosystem Engineering Journal

Journal homepage: <http://deej.kashanu.ac.ir>

Investigating Lagged Cross-correlation between Wind Erosion and Drought in Southern Iran's arid regions

Fatemeh Roustaei^{*1}, Zohre Ebrahimi-Khusfi², Mohammad Reza Kousari³, Mostafa Mokhtari⁴

Received: 14/06/2021

Accepted: 23/11/2021

Abstract

This study sought to detect the highest temporal correlation between wind erosion and drought in southern Iran's arid lands based on the Standardized Precipitation Index (SPI) and Standardized Dust Storm Index (SDSI) over a 50-year period (1965-2014). Using the Mann- Kendall test, changes in SPI (as a proxy of meteorological drought) and SDSI (as a proxy of wind erosion) trends were analyzed in temporal resolution (3, 6, 9, 12, 18, and 24 monthly time series). The wind erosion's response time to drought was estimated by Lagged cross-correlation. The results revealed a decreasing trend in the SPI time series, particularly in the long-term series (12, 18, and 24-month), and an increasing trend in the SDSI series in different time scales, from short-term to long-term series. These findings indicate the exacerbation of drought and wind erosion in the study region. Moreover, the cross-correlation analysis showed that the relationships between SPI and SDSI were negative at the level of 5% in all the time series. The maximum correlation was obtained from the cross-correlation between the 12-month SPI and 18-month SDSI without time lag ($R = -0.22$; $\alpha < 0.05$). These results indicated that in southern Iran's arid regions, changes in dust events had been affected by long-term drought. Therefore, it is expected that after long-term droughts, which considerably affect the soil moisture contents, the dust storms are intensified. The Finding of this research can help planners take necessary measures against sand and dust storm hazards.

Keywords: SDSI, Drought, Wind Erosion, Cross-Correlation, Soil Erosion.

1. Department of Nature Engineering, Faculty of Agriculture & Natural Resources, Ardakan University, Ardakan, Iran; froustaei@ardakan.ac.ir

2. Department of Ecological Engineering, Faculty of Natural Resources, University of Jiroft, Jiroft, Iran

3. Soil Conservation and Watershed Management Research Institute (SCWMRI), Tehran, Iran

4. Department Of Information Technology, Payame Noor University, Iran

DOI: 10.22052/JDEE.2021.242889.1074

1. Introduction

Defined as a prolonged period of low precipitation, drought leads to a severe reduction in water resources. In recent years, the severity and frequency of droughts have significantly increased in arid regions as a result of climate change (Chen et al., 2019), leading to a rapid reduction of surface flow (Martin et al., 2020), the drainage of groundwater reservoirs (Levy et al., 2020), exacerbated wind and water erosions, and changes in the land subsidence (Jeanne et al., 2019). Among these, wind erosion is a more serious environmental problem that has increased dust emissions and air pollution in most areas of the world (Duniway et al., 2019).

Strong winds can deflate the fertile topsoils and cause severe damage to biodiversity and various industries. In recent decades, soil erosion and drought have exerted adverse effects on the quality of humans lives and their health, crop yields, and the environment (Faraji et al., 2019, Cao et al., 2015, Atafar et al., 2019, Naderizadeh et al., 2016, Segovia et al., 2017, Gabbasova et al., 2016, Shen et al., 2020).

Wind erosion is considered one of the most important factors in land degradation in drylands (Duniway et al., 2019). Therefore, it is essential to evaluate the drought's impacts on wind erosion and manage their hazards over the arid regions worldwide.

Understanding how wind erosion events are influenced by droughts requires collecting long-term data and analyzing variations of different trends (Tegen & Schepanski, 2018). To this end, meteorological data can provide long-term information about wind erosion and droughts.

The dependence of wind erosion and dust events on climatic factors and droughts has been shown in numerous studies (Middleton, 2019, Achakulwisut et al., 2018, Bolles et al., 2019, Yarmoradi et al., 2020, Wang et al.,

2020). According to Pu et al. (2019), increased sand-dust activities in the U.S were mainly due to the decreased rainfall, increased surface winds velocity, and soil bareness. Sofue et al. (2018) reported the considerable effect of precipitation variations on dust storm events in the Gobi desert.

In this regard, increasing and decreasing trends of changes in the number of dusty days have been reported for Iran's eastern and northern regions, respectively, by Modarres & Sadeghi (2018). According to the Granger-Ramanathan averaging (GRA) method, the reason behind 65% of the seasonal changes occurred in the wind erosion events of the eastern half of Iran from 2000 to 2018 was the changes made in wind speed and vegetation (Ebrahimi-Khusfi et al., 2020). Taking the soil texture, topography map, and vegetation index (NDVI) into consideration, Nodej & Rezazadeh (2018) concluded that Hormozgan province could be a dust source., emphasizing that sensitivity to dust harvesting increases in warm seasons.

Numerous indices have been developed to evaluate droughts, enabling scientists to qualify the severity, frequency, and duration of the climatic anomalies. In this regard, the most common indicators include Palmer Drought Severity Index (PDSI), Effective Drought Index (EDI), Reconnaissance Drought Index (RDI), Standardized Precipitation-Evapotranspiration Index (SPEI), and Standardized Precipitation Index (SPI). However, precipitation is the only factor in all of these indicators, and SPI is known as a common drought index that is widely used for drought assessment (Wang et al., 2019, Paredes, 2016, Jasim & Awchi, 2020, Uddin et al., 2020).

Moreover, the activity level of wind erosion events can be evaluated via various indices, including the Aerosol Optical Index (Voss & Evan, 2019, Xian et al., 2020), remote sensing data, and meteorological data

concerning the frequency of dusty days (Yarmoradi et al., 2018). Nonetheless, as common meteorological data provide information about the frequency of dust events without analyzing their intensity, it is impossible to estimate wind erosion and its intensity through such data. By the way, considering the fact that the Dust Storm Index (DSI) can solve this problem by considering all dust events according to their potential in dust excavation, this index appears to be the most appropriate index for monitoring wind erosion and presenting the long-term intensity of dust events at moderate temporal resolution and at the regional spatial resolution based on meteorological observations (O'Loingsigh et al., 2015). Therefore, this study used DSI to analyze the trend of dust events.

Iran's water resources, especially the desert wetlands, have been severely damaged by droughts (Middleton, 2019). In general, Iran's arid/desert regions need to be investigated in terms of the droughts' effects on wind erosion, as important sources of dust emission, including the dried beds of Huorl-Azim, Bakhtegan, and Hamoun wetlands, the Lut and Kavir deserts, are located in these parts of Iran (Sardar Shahraki et al., 2020, Karimzadeh & Taghizadeh, 2019).

In recent years, dust storms have exacerbated living conditions in Iran's southern regions (Gerivani et al., 2011). According to Jalali & Davoudi (2008), factors such as little precipitation in south and southwest regions, drought, decreasing water levels in lagoons and ponds, the withering of desert plants, and subsequently rising winds since February and March 2007 onwards have led to 20 to 30 percent increase in the regions' dust storms. However, while changes in wind erosion phenomena across Iran's arid regions have been previously studied (Ebrahimi-

Khusfi et al., 2020, Ebrahimi Khusfi et al., 2020), its temporal response to meteorological drought in southern Iran's arid regions has not been investigated. To this end, this study used the standardized dust storm index (SDSI) for the first time to analyze the trend of changes in dust storms. Moreover, the time lag between drought and wind erosion was investigated via cross-correlation analysis in various time series (from three to twenty-four months) of SPI and SDSI over a long-term period (1965-2014).

In total, this study was conducted with the following objectives:

(I) To investigate the trend of temporal changes in the SPI (as a proxy of meteorological drought) and SDSI (as a proxy of wind erosion activities or dust storms) over the south of Iran.

(II) To determine the relationship between SPI and SDSI in different time series.

(III) To analyze the temporal response of wind erosion to drought in different time lags.

2. Materials and Methods

2.1. The Study area

The study area includes southern Iran's arid region, which is about 936980 km² and, located at the latitude of 26°00'N to 31°39'N and the longitude of 44°00'E to 63°00'E (Fig. 1). The average elevation of the region and the mean annual precipitation is 857.3 m and 137 mm, respectively. As the area is prone to wind erosion, its sand dunes and dried salt lakes are mainly distributed in its southeast and southwest parts (Rashki et al., 2017, Abbasi et al., 2019). Furthermore, different soil types, including salt-marsh soil, Gypsum soils, saline-alluvial soils, Sierozem, and regosols, could be observed in this area (Roozitalab et al., 2018).

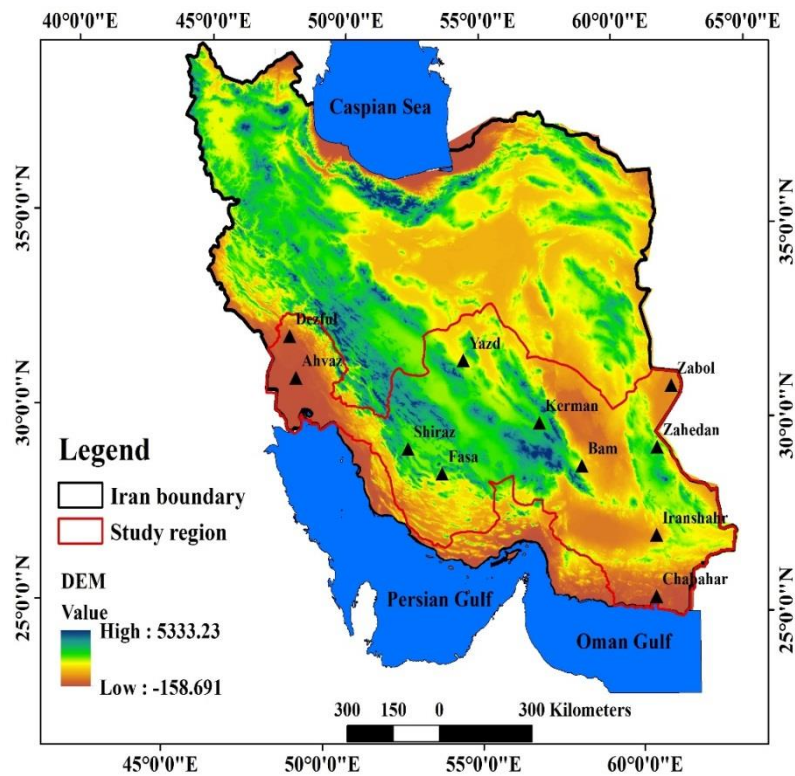


Figure (1): Geographical distribution map of synoptic stations in southern Iran

The total number of synoptic stations with relatively good distribution and long-term data

(1965-2014) in this area is 11 stations, the characteristics of which are presented in table 1.

Table (1): Geographical coordinates and elevation of the selected stations in this study

Synoptic station	Longitude	Latitude	Elevation (m)
Yazd	31.9	54.2	1230.2
Ahvaz	31.3	48.7	22.5
Bam	29.1	58.3	1066.9
Chabahar	25.2	60.6	8
Dezful	32.4	48.3	143
Fasa	28.8	53.7	1268
Iranshahr	27.2	60.7	591.1
Kerman	30.2	56.9	1754
Shiraz	29.5	52.6	1488
Zabol	31.1	61.5	489.2
Zahedan	29.4	60.9	1370

2.2. Methodology

Figure 2 shows the main steps followed in this study. In short, after obtaining the precipitation and wind speed data, SPI and SDSI indices were calculated. Then, trend changes in drought and wind erosion indices were

determined via the Mann-Kendall test. Finally, the relationship between SDSI and SPI time series was examined through the cross-correlation test. Further details of the research methodology are presented in the following sub-sections.

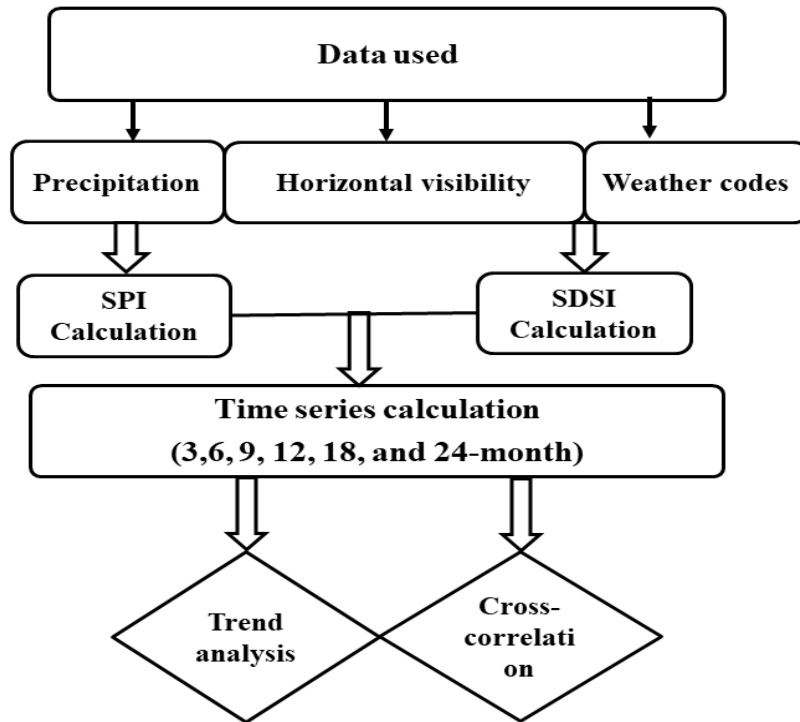


Figure (2): Flowchart of this study's methodology

2.2.1. Data sets

The required data regarding precipitation, dust codes, wind speed, and horizontal visibility were obtained on a 3-hourly time scale for the 1965-2014 period from the Iranian Meteorological Organization (IRIMO). Also, the rainfall data was used to calculate the SPI index, and other data were used to calculate the SDSI, as described in the following sections.

2.2.2. Meteorological drought estimation

The Standardized Precipitation Index (SPI) was first proposed by McKee et al. (1993) as a meteorological drought index. Explaining the drought on various time scales, this index is based on the rainfall data, and its value is not affected by the regional geography. These features distinguish the SPI from the other indices (Belayneh & Adamowski, 2012).

SPI is calculated by performing a gamma distribution via the following equation:

$$\Gamma(\alpha) = \int_0^{\infty} y^{\alpha-1} e^{-y} dy \tag{1}$$

where $\Gamma(\alpha)$ is the gamma function, and α stands for the shape factor that is calculated using equation (2).

There are different techniques for estimating these two parameters. For instance, Edwards & McKee (1997) proposed a method for calculating the maximum likelihood-based on equations (2):

$$\alpha = 0.25B(\sqrt{1 + 1.33B} + 1) \tag{2}$$

where

$$B = \ln(\bar{P}) - \frac{\sum \ln(P)}{n} \tag{3}$$

where n refers to the total number of observations, and P indicates the precipitation amounts.

The cumulative probability of P values and Gamma function can be calculated through equations (4) and (5), respectively:

$$K(p) = \int_0^x k(P)dx = \frac{1}{\beta^\alpha \Gamma(\alpha)} = \int_0^x P^{(\alpha-1)} e^{(-P/\beta)} \tag{4}$$

$$M(p) = a + (1 - a)K(p) \tag{5}$$

where "a" is the probability of zero precipitation, and $M(p)$ refers to the cumulative probability. The SPI index is then computed as the following:

$$Z = SPI = \begin{cases} -\left(t - \frac{c_0+c_1t+c_2t^2}{1+d_1t+d_2t_1^2+d_3t^3}\right) & \text{for } 0 < M(p) \leq 0.5 \\ +\left(t - \frac{c_0+c_1t+c_2t^2}{1+d_1t+d_2t_1^2+d_3t^3}\right) & \text{for } 0.5 < M(p) < 1 \end{cases} \quad (6)$$

where "t" factor is defined as follows:

$$t = \begin{cases} \sqrt{\ln \left[\frac{1}{(M(p))^2} \right]} & \text{for } 0 < M(p) \leq 0.5 \\ \sqrt{\ln \left[\frac{1}{(1-M(p))^2} \right]} & \text{for } 0.5 < M(p) < 1 \end{cases} \quad (7)$$

where "x" refers to the cumulative probability of recorded rainfall, and c0, c1, c2, d0, d1, d2 indicate constants values (Mishra & Desai, 2005).

Positive and negative values of this index indicate dry and wet years with different intensities, respectively. Moreover, the monthly SPI values were calculated for various time scales (3, 6, 9, 12, 18, 24 and, 48 months) based on what was described above.

3.3 SDSI calculation

Dust Storm Index (DSI) is a useful index for long-term monitoring of wind erosion events (O’Loingsigh et al., 2014), which is

calculated by Leys et al. (2011) based on dust concentration during local dust events (LDE), moderate dust storm (MDS), severe dust storms (SDS), and field observations. DSI is computed using equation (8), and its value is greater than or equal to zero. Higher values of this index suggest more soil losses and intensification of wind erosion events.

$$DSI_m = \sum_{i=1}^n \left[(5 \times SDS) + MDS + \left(\frac{LDE}{20}\right) \right] \quad (8)$$

In the above equation, "n" shows the number of stations, and "i" is the value of "n" stations for $i=1-n$. Also, LDE, MDS, and SDS are local, moderate, and severe dust storms, respectively.

Table 2 describes the definitions of weather codes offered by the World Meteorological Organization (WMO). Codes (07-08), (09, 30 to 32), and (33 to 35) demonstrate LDE, MDS, and SDS, respectively.

Finally, the DSI- related values were standardized using the method described for the drought index, and the standardized dust storm index (SDSI) values were calculated for different time series.

Dust storm type	code	definition
Local dust events	07	Deflated sand and dust
	08	Dust devils
Moderate dust storm	09	dust incidents occurred near the station in the past hours
	30	Declined slight and moderate DE with 0.2m <HV <1Km
	31	Constant slight and moderate DE with 0.2m <HV <1Km
	32	Rising slight and moderate DE with 0.2m <HV <1Km
Severe dust storm	33	Declined SDS with H.V. <200 m
	34	Stable SDS with H.V. <200 m
	35	Rising SDS with H.V. <200 m

Table (2): WMO⁵ codes relating to wind erosion

ΔWorld Meteorological Organization

2.2.3. Mann-Kendall test

The Mann-Kendall is a non-parametric test widely utilized to detect the trend of changes in various variables. The zero hypothesis (H0) belongs to independent data with a definite distribution. An alternative hypothesis (H.A.) indicates that the data follows a uniform trend. The Mann-Kendall statistic Z_m is given in terms of equations (9) to (12):

$$S = \sum_{i=1}^{n-1} \sum_{j=i+1}^n \text{sgn}(x_j - x_i) \tag{9}$$

$$\text{sgn}(x_j - x_i) = \begin{cases} +1 & \text{if } (x_j - x_i) > 0 \\ 0 & \text{if } (x_j - x_i) = 0 \\ -1 & \text{if } (x_j - x_i) < 0 \end{cases} \tag{10}$$

$$\text{VAR}(S) = \frac{1}{18} \left[n(n-1)(2n+5) - \sum_{p=1}^q t_p(t_p-1)(2t_p+5) \right] \tag{11}$$

$$Z_m = \begin{cases} \frac{S-1}{\sqrt{\text{VAR}(S)}} & \text{if } S > 0 \\ 0 & \text{if } S = 0 \\ \frac{S+1}{\sqrt{\text{VAR}(S)}} & \text{if } S < 0 \end{cases} \tag{12}$$

where "n" and "m" are the number of observations and interconnected groups, respectively. "xi" and "xj" indicate the values of the study variables in years "i" and "j" (j>i), and "sgn" refers to sing (+ or -) of (xj - xi). Moreover, "Z" refers to the standard test statistic. The positive values of "Z" suggest upward trends, whereas negative "Z" values demonstrate downward trends. A significance level "α" is also applied to assessing either an upward or downward trend. to this end, this study applied a 5% significance level (alpha=5%). The Durbin–Watson test was also administered as a usual method for autocorrelation testing. For more details, see

Ahani et al. (2012). Backward correlation refers to the correlation between two time series transmitted in relation to each other.

2.2.4. Cross-Correlation analysis

Lagged correlation shows the dependence of two time series on each other by considering different delay times. For different input data, the cross-correlation function relates to the thump reaction. In the asymmetrical cross-correlation function, the output signal is affected by the output signal. Response time is defined as the delay associated with the maximum correlation function (Lee et al., 2006). At a given delay time, the cross-correlation is obtained from equation (13) (McCoy & Blanchard, 2008):

$$r_t = \frac{n^* \sum p_1 p_2 - \sum p_1 \sum p_2}{\sqrt{[n^* \sum p_1^2 - (\sum p_1)] [n^* \sum p_2^2 - (\sum p_2)]}} \tag{13}$$

where "r_t" is the cross-correlation coefficient at lag time t; "t" refers to the time lag between study time series; "n*" shows the number of overlapping data; "p₁" is the SPI series, and "p₂" shows the dust storm series. It should be noted that if "r_t" values are larger than the standard error, the correlation value with a specified lag time is significant at the 5% confidence level (Lee et al., 2006).

3. Results and Discussion

Figures 3 and 4 show the SPI and SDSI time series at different time scales (3, 6, 9, 12, 18, and 24 monthly) for southern Iran's region over the study period (1965-2014), respectively. In these Figures, the first-order linear trends for each time series are displayed with red lines. According to this study's results, the trend of SPI changes has been decreasing in all the time series mentioned (Fig. 3). The results obtained from the M.K. test indicate that the SPI's downward trend was significant at time scales of 9, 12, 18, and 24-month (Table 3). The Z values for these time

scales were estimated as -2.20, -2.80, -3.68, and -4.55, respectively. These findings suggest that more severe droughts have dominated the arid lands of southern Iran in recent years, particularly in the mentioned time scales. In contrast, the SDSI variations had an increasing trend in all time scales (Fig. 4). The estimated Z values were more than + 10 over the whole study period (from 3 to 24-month) (Table 3), showing that dust storms have been intensified

in the study region throughout the study period.

The study's results also revealed that there was a negative correlation between the absolute value of the Z and SPI and SDSI values. In other words, with the decrease of drought trend (an increase of SPI values) in Iran's southern regions, the rate of dust storms had decreased and vice versa.

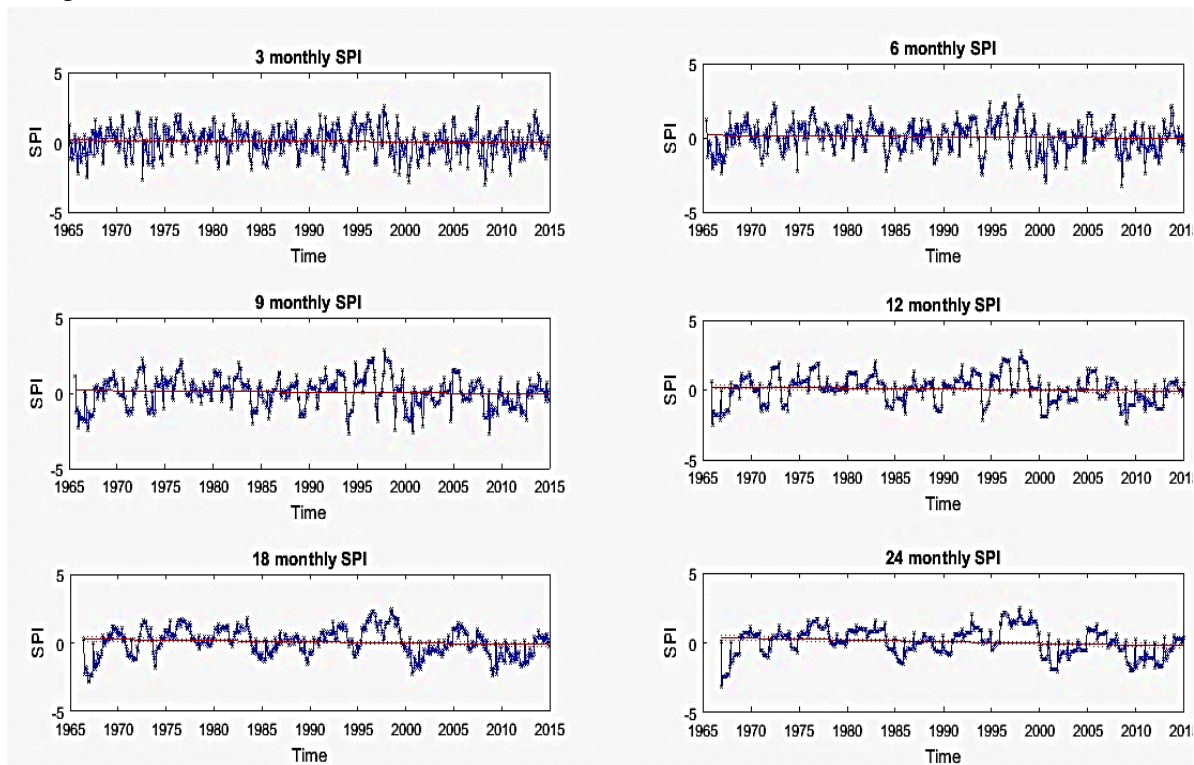


Figure (3): SPI variations in different time series for the Southern regions of Iran during 1965-2014

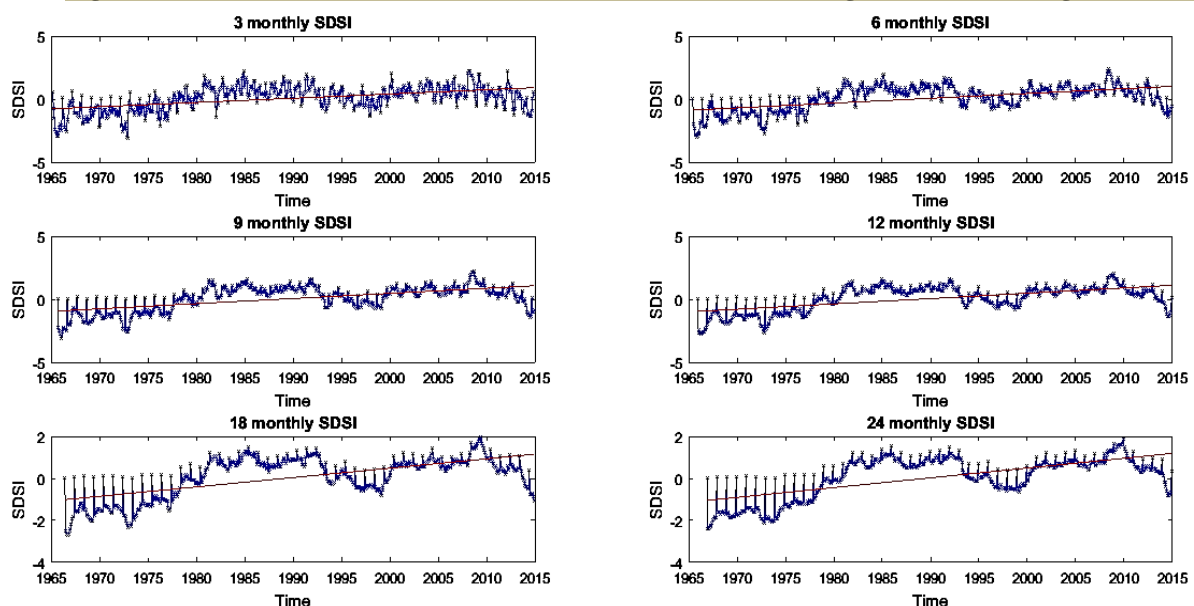


Figure (4): SDSI variations in different time series for Iran's Southern regions during 1965-2014

	Time Series	3 Monthly	6 Monthly	9 Monthly	12 Monthly	18 Monthly	24 Monthly
Z parameter	SPI	-1.2665	-1.67	-2.20*	-2.80*	-3.68*	-4.55*
	SDSI	11.85*	12.77*	13.40*	13.78*	13.94*	14.39*

Table (3): Mann- Kendall statistic values in different time series of SDSI (Z- value > +1.96 and <-1.96 represent upward and downward trends, respectively. * indicates a significant level at $\alpha<0.05$)

Moreover, the effects of different time-lags on SPI and SDSI time series were investigated using Lagged cross-correlation analysis. Table 4 shows the estimates made in this regard. In this table, the row "a" is the first time-lag when there was a significant correlation between SPI and SDSI time series; the row "b" is the time-lag when the highest correlation was observed, and the row "c" indicates the maximum correlation coefficients between SPI and SDSI time series in the time-lag with maximum correlation coefficients. For instance, the results obtained from the cross-correlation between the 3-month SPI and 18-

month SDSI show that from the fifth time-lag on, the relationship between these time series has become significant and that in the thirteenth time-lag, the correlation coefficient has been maximized. Accordingly, the respective plot can be seen in figure 5(a), as shown in Table IV and figure 5(b). Furthermore, the maximum correlation was found between 18-month SPI and 12-month SDSI without any time lag ($R= -0.22$; $p <0.05$). The study's results also revealed that the correlation coefficients between long-term series are often higher than the short-term ones.

		Standardized Dust Storm Index (SDSI)							
		3	6	9	12	18	24		
Standardized Precipitation Index (SPI)	3	1	1	3	5	5	0	The first lag with significant r	a
		3	5	8	8	13	14	The lag with maximum r	b
		-0.12	-0.13	-0.14	-0.14	-0.15	-0.15	The maximum r	c
	6	0	1	0	0	1	0	The first lag with significant r	a
		2	5	6	7	10	12	The lag with maximum r	b
		-0.16	-0.16	-0.16	-0.17	-0.18	-0.17	The maximum r	c
	9	0	0	1	0	0	0	The first lag with significant r	a
		0	2	4	6	7	9	The lag with maximum r	b
		-0.19	-0.18	-0.16	-0.17	-0.18	-0.17	The maximum r	c
	12	0	0	0	0	0	0	The first lag with significant r	a
		0	0	2	5	7	7	The lag with maximum r	b
		-0.19	-0.20	-0.19	-0.18	-0.19	-0.20	The maximum r	c
18	0	0	0	0	0	0	The first lag with significant r	a	
	0	1	0	0	5	7	The lag with maximum r	b	
	-0.19	-0.20	-0.21	-0.22	-0.19	-0.20	The maximum r	c	
24	0	0	0	0	0	0	The first lag with significant r	a	
	0	0	0	1	1	3	The lag with maximum r	b	
	-0.19	-0.21	-0.22	-0.22	-0.22	-0.20	The maximum r	c	

Table (4): Lag cross-correlation matrix of SPI and SDSI over the Southern regions of Iran (significant level is $\alpha<0.05$)

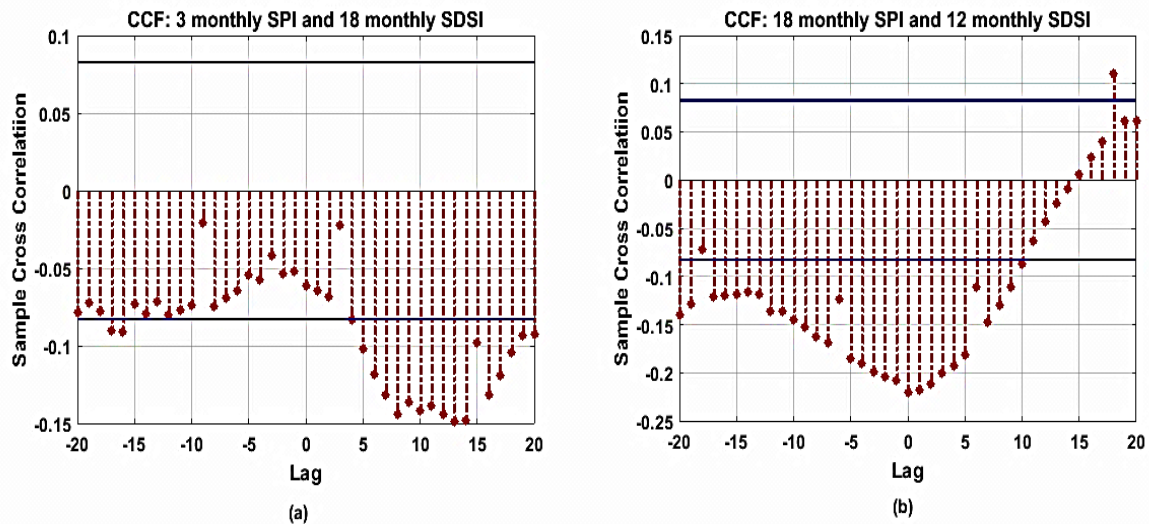


Figure (5): The time-lag cross-correlation between SPI and SDSI over Iran's Southern regions. Significant levels are ($p < 0.05$) displayed by blue horizontal lines

In total, the study's findings indicated that the study region experienced a significant downward trend in SPI and a significant upward trend in SDSI over the monitoring period (1965-2014). The exacerbation of meteorological droughts has been reported in many previous studies (Moradi Dashtpajardi et al., 2014), which is consistent with the present study's findings. The intensification of dust storms in Iran has also been approved by Ebrahimi Khusfi et al., 2020a, and Vali & Roustaei, 2018. The results of this study also suggested that while the significant increasing trend in SDSI had occurred over the whole time series of the study period, the significant decreasing trend in SPI had mainly occurred in the long-term series. Considering the fact that low precipitation rate is one of the special features of the drylands, especially at short-term scales (e.g., one-to-three-month time scales), it can be concluded that with an increase in time series, precipitation variations become more significant and meaningful (Kangas & Brown, 2007). In other words, the existence of so many zeros in the precipitation time series causes the data not to follow the normal distribution, and the accuracy of SPI values decreases in the short-term series compared to what occurs in the long-term

series (Ahani et al., 2012).

Although there was a significant negative correlation between SPI and SDSI values in southern Iran's arid regions at different time series, the highest correlation coefficients were found between the 18-month SPI and the 12-month SDSI series (-0.22) with zero time-lag (Table 4). The significant negative correlation between precipitation and dust storms has been reported in some previous studies (Zender & Kwon, 2005, McTainsh et al., 1989, Mahowald et al., 2003, Guan et al., 2015), which confirm this study's results. Therefore, it is expected that after long-term droughts that considerably affect the soil moisture contents, the dust storms are intensified. On the other hand, rainfall has a critical role in controlling wind erosion events in arid and semi-arid regions because it is one of the major sources of ground moisture increase (Chen et al., 2020).

Moreover, as rainfall and soil moisture decrease, the dryness of the earth's surface increases, and the resistance of soil to wind shear decreases. Therefore, the soil is easily removed from the bed, leading to the formation of sand and dust storms (Ebrahimi Khusfi et al., 2020). In arid regions, sparse vegetation may be another factor in reducing

the time lag between drought and wind erosion events since vegetation is an important factor in maintaining the soil's moisture and protecting the soil against wind erosion. In other words, vegetation helps increase the wind erosion response time to droughts (Wang et al., 2003, Capodici et al., 2008). Therefore, it appears that the simultaneous occurrence of wind erosion and drought in the study area is due to the large amounts of wind erosion-sensitive lands (e.g., the Lut and Kavir deserts and the wetland dried beds, Sistan Hamouns, Jazmurian dried lake) compared to the vegetated lands.

4. Conclusion

This study sought to investigate the relationship between drought and dust storms at various time series based on meteorological data obtained from several stations across Iran's southern regions. To this end, SPI and SDSI trends were investigated using the non-parametric M.K. test at different time scales (3, 6, 9, 12, 18, 24 monthly time series) over a 50-year period (1965-2014). The study's findings showed that the study region experienced significant downward trends in SPI, which indicates an increase in drought, and significant upward trends in SDSI, which demonstrates a decrease in wind erosion.

References

1. Abbasi, H., Opp, C., Groll, M., Rohipour, H. and Gohardoust, A., 2019. Assessment of the distribution and activity of dunes in Iran based on mobility indices and ground data, *Aeolian Research*, 41: 100539.
2. Achakulwisut, P., Mickley, L. and Anenberg, S., 2018. Drought-sensitivity of fine dust in the US Southwest: Implications for air quality and public health under future climate change, *Environmental Research Letters*, 13: 054025.
3. Ahani, H., Kherad, M., Kousari, M. R., Rezaeian-Zadeh, M., Karampour, M. A., Ejraee, F. and Kamali, S., 2012. An investigation of trends in precipitation volume for the last three decades in different regions of Fars province, Iran, *Theoretical and Applied Climatology*, 109: 361-382.
4. Atafar, Z., Pourpak, Z., Yunesian, M., Nicknam, M. H., Hassanvand, M. S., Soleimanifar, N., Saghafi, S., Alizadeh, Z., Rezaei, S., Ghanbarian, M., Ghoskhal, M. G., Osornio-Vargas, A. R. and Naddafi, K., 2019. Proinflammatory effects of dust storm and thermal inversion particulate matter (PM10) on human peripheral blood mononuclear cells (PBMCs) in vitro: a comparative approach and analysis, *Journal of Environmental Health Science and Engineering*, 17: 433-444.
5. Belayneh, A. and Adamowski, J., 2012. Standard Precipitation Index Drought Forecasting Using Neural Networks, Wavelet Neural Networks, and Support Vector

As expected, according to the cross-correlation analysis, the increase in drought intensity has exacerbated soil erosion in southern Iran. Given that the leading cause of the decrease in rainfall, as the most important factor affecting meteorological drought, is an increase in greenhouse gases derived from increasing human activities (Şahin et al., 2019), taking appropriate measures can mitigate the negative effects of drought on other phenomena, particularly dust storms. The development of plants that are resistant to climate stress, especially drought stress, may minimize the risks of wind erosion and dust storms in arid areas. Thus, such measures can reduce greenhouse gas emissions, increase the soil's moisture-holding capacity and decrease the number of dust storms.

Moreover, investigating and discovering the temporal response of dust storms to other climatic and terrestrial factors in different regions can provide a broader insight into wind erosion and identify the impact time of the factors affecting it, which is recommended for future studies. Also, predicting the temporal trends of these factors using new models and techniques of machine-learning can be another suitable approach to find out their future changes and take measures in line with combat to desertification goals.

- Regression, *Applied Computational Intelligence and Soft Computing*, 6: 794061.
6. Bolles, K., Sweeney, M. and Forman, S., 2019. Meteorological catalysts of dust events and particle source dynamics of affected soils during the 1930s Dust Bowl drought, Southern High Plains, USA, *Anthropocene*, 27: 100216.
 7. Cao, H., Liu, J., Wang, G., Guang, Y. and Luo, L., 2015. Identification of sand and dust storm source areas in Iran, *Journal of Arid Land* volume, 7 :567–578.
 8. Capodici, F., Ciraolo, G., La Loggia, G., Liuzzo, L., Noto, L. and Noto, M., 2008. Time series analysis of climate and vegetation variables in the Oreto watershed, *European Water*, 23: 133-145.
 9. Chen, L., Chen, X., Cheng, L., Zhou, P. and Liu, Z., 2019. Compound hot droughts over China: Identification, risk patterns and variations, *Atmospheric Research*, 227: 210-219.
 10. Chen, W., Li, Z., Jiao, L., Wang, C., Gao, G. and Fu, B., 2020. Response of Soil Moisture to Rainfall Event in Black Locust Plantations at Different Stages of Restoration in Hilly-gully Area of the Loess Plateau, China, *Chinese Geographical Science*, 30: 427-445.
 11. Duniway, M. C., Pfennigwerth, A. A., Fick, S. E., Nauman, T. W., Belnap, J. and Barger, N. N., 2019. Wind erosion and dust from US drylands: a review of causes, consequences, and solutions in a changing world, *Ecosphere*, 10: e02650.
 12. Ebrahimi-Khusfi, Z., Taghizadeh-Mehrjardi, R. and Mirakbari, M., 2020. Evaluation of machine learning models for predicting the temporal variations of dust storm index in arid regions of Iran, *Atmospheric Pollution Research*.
 13. Ebrahimi Khusfi, Z., Roustaei, F., Ebrahimi Khusfi, M. and Naghavi, S., 2020. Investigation of the relationship between dust storm index, climatic parameters, and normalized difference vegetation index using the ridge regression method in arid regions of Central Iran, *Arid Land Research and Management*, 34: 239-263.
 14. Edwards, D. C. and McKee, T. B. 1997. Characteristics of 20th century drought in the United States at multiple time scales. DTIC Document.
 15. Faraji, M., Pourpak, Z., Naddafi, K., Nodehi, R. N., Nicknam, M. H., Shamsipour, M., Osornio-Vargas, A. R., Hassanvand, M. S., Alizadeh, Z. and Rezaei, S., 2019. Chemical composition of PM 10 and its effect on in vitro hemolysis of human red blood cells (RBCs): a comparison study during dust storm and inversion, *Journal of Environmental Health Science and Engineering*, 17: 493-502.
 16. Gabbasova, I. M., Suleimanov, R. R., Khabirov, I. K., Komissarov, M. A., Fruehauf, M., Liebelt, P., Garipov, T. T., Sidorova, L. V. and Khaziev, F. K., 2016. Temporal changes of eroded soils depending on their agricultural use in the southern Cis-Ural region, *Eurasian Soil Science*, 49: 1204-1210.
 17. Gerivani, H., Lashkaripour, G. R., Ghafoori, M. and Jalali, N., 2011. The source of dust storm in Iran: a case study based on geological information and rainfall data, *Carpathian Journal of Earth and Environmental Sciences*, 6.
 18. Guan, Q., Yang, J., Zhao, S., Pan, B., Liu, C., Zhang, D. and Wu, T., 2015. Climatological analysis of dust storms in the area surrounding the Tengger Desert during 1960–2007, *Climate dynamics*, 45: 903-913.
 19. Jalali, N. and Davoudi, M., 2008. Inspecting the origins and causes of the dust storms in the Southwest and West parts of Iran and the regions affected, Internal reports of Soil Conservation and Watershed anagement Research Institute (SCWMRI), Iran.
 20. Jasim, A. I. and Awchi, T. A., 2020. Regional meteorological drought assessment in Iraq, *Arabian Journal of Geosciences*, 13: 284.
 21. Jeanne, P., Farr, T. G., Rutqvist, J. and Vasco, D. W., 2019. Role of agricultural activity on land subsidence in the San Joaquin Valley, California, *Journal of hydrology*, 569: 462-469.
 22. Kangas, R. S. and Brown, T. J., 2007. Characteristics of US drought and pluvials from a high-resolution spatial dataset, *International Journal of Climatology*, 27: 1303-1325.
 23. Karimzadeh, S. and Taghizadeh, M., 2019. Potential of dust emission resources using small wind tunnel and GIS: case study of Bakhtegan playa, Iran, *Applied Water Science*, 9.
 24. Lee, L. J. E., Lawrence, D. S. L. and Price, M., 2006. Analysis of water-level response to rainfall and implications for recharge pathways in the Chalk aquifer, SE England, *Journal of Hydrology*, 330: 604-620.
 25. Levy, Z. F., Fram, M. S., Faulkner, K. E., Alpers, C. N., Soltero, E. M. and Taylor, K. A., 2020. Effects of montane watershed development on vulnerability of domestic groundwater supply during drought, *Journal of Hydrology*, 583: 124567.
 26. Leys, J. F., Heidenreich, S. K., Strong, C. L.,

- McTainsh, G. H. and Quigley, S., 2011. PM10 concentrations and mass transport during “Red Dawn”–Sydney 23 September 2009, *Aeolian Research*, 3: 327-342.
27. Mahowald, N. M., Bryant, R. G., del Corral, J. and Steinberger, L., 2003. Ephemeral lakes and desert dust sources, *Geophysical Research Letters*, 30.
28. Martin, J. T., Pederson, G. T., Woodhouse, C. A., Cook, E. R., McCabe, G. J., Anchukaitis, K. J., Wise, E. K., Erger, P. J., Dolan, L., McGuire, M., Gangopadhyay, S., Chase, K. J., Littell, J. S., Gray, S. T., St. George, S., Friedman, J. M., Sauchyn, D. J., St-Jacques, J.-M. and King, J., 2020. Increased drought severity tracks warming in the United States’ largest river basin, *Proceedings of the National Academy of Sciences*, 117: 11328-11336.
29. McCoy, K. J. and Blanchard, P. J. 2008. Precipitation, Ground-water Hydrology, and Recharge Along the Eastern Slopes of the Sandia Mountains, Bernalillo County, New Mexico. *Scientific Investigations Report*. Version 1.0 ed.
30. McKee, T. B., Doesken, N. J. and Kleist, J., The relationship of drought frequency and duration to time scales. *Proceedings of the 8th Conference on Applied Climatology*, 1993: American Meteorological Society Boston, MA, USA, 179-183.
31. McTainsh, G. H., Burgess, R. and Pitblado, J. R., 1989. Aridity, drought and dust storms in Australia (1960–84), *Journal of Arid Environments*, 16: 11-22.
32. Middleton, N., 2019. Variability and Trends in Dust Storm Frequency on Decadal Timescales: Climatic Drivers and Human Impacts, *Geosciences*, 9: 261.
33. Mishra, A. and Desai, V., 2005. Drought forecasting using stochastic models, *Stochastic Environmental Research and Risk Assessment*, 19: 326-339.
34. Modarres, R. and Sadeghi, S., 2018. Spatial and temporal trends of dust storms across desert regions of Iran, *Natural Hazards*, 90: 101-114.
35. Moradi Dashtpajardi, M., Kousari, M. R., Vagharfard, H., Ghonchepour, D., Hosseini, M. E. and Ahani, H., 2014. An investigation of drought magnitude trend during 1975–2005 in arid and semi-arid regions of Iran, *Environmental Earth Sciences*, 73: 1231-1244.
36. Naderizadeh, Z., Khademi, H. and Ayoubi, S., 2016. Biomonitoring of atmospheric heavy metals pollution using dust deposited on date palm leaves in southwestern Iran, *Atmósfera*, 29: 141-155.
37. Nodej, T. M. and Rezazadeh, M., 2018. The spatial distribution of critical wind erosion centers according to the dust event in Hormozgan province (south of Iran), *CATENA*, 167: 340-352.
38. O’Loingsigh, T., McTainsh, G. H., Tews, E. K., Strong, C. L., Leys, J. F., Shinkfield, P. and Tapper, N. J., 2014. The Dust Storm Index (DSI): A method for monitoring broadscale wind erosion using meteorological records, *Aeolian Research*, 12: 29-40.
39. Paredes, F. J., 2016. A probabilistic model for the prediction of meteorological droughts in Venezuela, *Atmósfera*, 29: 311-323.
40. Pu, B., Ginoux, P., Kapnick, S. B. and Yang, X., 2019. Seasonal Prediction Potential for Springtime Dustiness in the United States, *Geophysical Research Letters*, 46: 9163-9173.
41. Rashki, A., Arjmand, M. and Kaskaoutis, D., 2017. Assessment of dust activity and dust-plume pathways over Jazmurian Basin, southeast Iran, *Aeolian Research*, 24: 145-160.
42. Roozitalab, M. H., Siadat, H. and Farshad, A. 2018. *The soils of Iran*, Springer.
43. Şahin, Ü. A., Onat, B. and Ayyavaz, C. 2019. Climate Change and Greenhouse Gases in Turkey. *Recycling and Reuse Approaches for Better Sustainability*. Springer.
44. Sardar Shahraki, A., Shahraki, J. and Hashemi Monfared, S. A., 2020. An integrated model for economic assessment of environmental scenarios for dust stabilization and sustainable flora–fauna ecosystem in international Hamoun wetland, *Environment, Development and Sustainability*.
45. Segovia, C., Gómez, J. D., Gallardo, P., Lozano, F. J. and Asensio, C., 2017. Soil nutrients losses by wind erosion in a citrus crop at southeast Spain, *Eurasian Soil Science*, 50: 756-763.
46. Shen, H. O., Wang, D. L., Wen, L. L., Zhao, W. T. and Zhang, Y., 2020. Soil Erosion and Typical Soil and Water Conservation Measures on Hillslopes in the Chinese Mollisol Region, *Eurasian Soil Science*, 53: 1509-1519.
47. Sofue, Y., Hoshino, B., Demura, Y., Kai, K., Baba, K., Nduati, E., Kondoh, A. and Sternberg, T., 2018. Satellite Monitoring of Vegetation Response to Precipitation and Dust Storm Outbreaks in Gobi Desert Regions, *Land*, 7: 19.
48. Tegen, I. and Schepanski, K., 2018. Climate Feedback on Aerosol Emission and Atmospheric Concentrations, *Current Climate Change Reports*, 4: 1-10.

49. Uddin, M. J., Hu, J., Islam, A. R. M. T., Eibek, K. U. and Nasrin, Z. M., 2020. A comprehensive statistical assessment of drought indices to monitor drought status in Bangladesh, *Arabian Journal of Geosciences*, 13: 323.
50. Voss, K. and Evan, A., 2019. A New Satellite-Based Global Climatology of Dust Aerosol Optical Depth, *Journal of Applied Meteorology and Climatology*, 59.
51. Wang, J., Rich, P. and Price, K., 2003. Temporal responses of NDVI to precipitation and temperature in the central Great Plains, USA, *International Journal of Remote Sensing*, 24: 2345-2364.
52. Wang, Q., Liu, Y.-y., Zhang, Y.-z., Tong, L.-j., Li, X., Li, J.-l. and Sun, Z., 2019. Assessment of Spatial Agglomeration of Agricultural Drought Disaster in China from 1978 to 2016, *Scientific reports*, 9: 1-8.
53. Wang, X., Hua, T. and Che, H., 2020. Temporal variation of dust aerosol pollution in northern China, *Arabian Journal of Geosciences*, 13: 108.
54. Xian, P., Klotzbach, P. J., Dunion, J. P., Janiga, M. A., Reid, J. S., Colarco, P. R. and Kipling, Z., 2020. Revisiting the Relationship between Atlantic Dust and Tropical Cyclone Activity using Aerosol Optical Depth Reanalyses: 2003-2018, *Atmos. Chem. Phys. Discuss.*, 2020: 1-43.
55. Yarmoradi, Z., Nasiri, B., Karampour, M. and Mohammadi, G. H., 2018. Trend analysis of dusty days frequency in Eastern parts of Iran associated with Climate Fluctuations, *Desert Ecosystem Engineering Journal*, 7: 1-14.
56. Yarmoradi, Z., Nasiri, B., Mohammadi, G. H. and Karampour, M., 2020. Long-term characteristics of the observed dusty days and its relationship with climatic parameters in East Iran, *Arabian Journal of Geosciences*, 13: 242.
57. Zender, C. S. and Kwon, E. Y., 2005. Regional contrasts in dust emission responses to climate, *Journal of Geophysical Research: Atmospheres*, 110: D13201.